Microscopic nature of coordination defects in amorphous silicon

Martin Stutzmann
Max-Planck-Institut für Festkörperforschung, Heisenbergstrasse 1, Postfach 80 06 65, D-7000 Stuttgart 80, Federal Republic of Germany

David K. Biegelsen
Xerox Corporation, Palo Alto Research Center, Palo Alto, California 94304
(Received 9 June 1989)

^{29}Si spectra of the $g=2.0055$ spin resonance in undoped hydrogenated amorphous silicon containing the natural abundance of the ^{29}Si isotope have been measured with a sufficient signal-to-noise ratio to allow a quantitative modeling of the underlying hyperfine and g tensors. These experimental results are used to discuss the microscopic origin of the main deep electronic defect state in a-Si.

I. INTRODUCTION

It is well established that the electronic properties of hydrogenated amorphous silicon (a-Si:H) are strongly influenced by a dominant localized defect level in the mobility gap of this material. This electronic defect essentially determines the lifetime of excess charge carriers in undoped a-Si:H and, consequently, limits the performance of a-Si:H thin films for many applications. The fingerprint of this defect is a characteristic electron-spin resonance signal with a g value $g=2.0055$,[1,2] which is generally observed in undoped a-Si and a-Si:H, and whose intensity can be used as a convenient measure for the quality of a given amorphous silicon specimen.

As far as the microscopic origin of this defect and of the $g=2.0055$ resonance is concerned, until recently it was more or less tacitly assumed that this defect state was that of a threefold-coordinated, neutral silicon atom $Si^0_{(3)}$, whose fourth atomic sp^3 hybrid orbital had remained unbonded because of the lack of bonding partners in a heavily distorted network such as a-Si:H. Consequently, the resulting electronic defect level was given the descriptive name "dangling bond," in analogy to similar defect states at surfaces or grain boundaries of crystalline silicon.[3,4] In fact, for most properties of a-Si:H, the microscopic origin of the $g=2.0055$ defect level is much less important than the energy position in the gap and the dependence of the defect density on deposition parameters. During the past few years, however, there have been more and more attempts to describe the macroscopic electronic properties of device-grade a-Si:H within the framework of unifying microscopic structural models, such as the negative-U model,[5,6] the thermal equilibration model,[7,8] or the weak-bond dangling-bond conversion model.[9,10] The common point of all of these microscopic pictures is that they rely to a certain extent on an as-yet unproven hypothesis, namely, that the dominant structural defect in a-Si:H is indeed the silicon dangling bond.

It is, therefore, understandable that in 1986 Pantelides attracted a considerable amount of attention when he proposed that not Si dangling bonds, but instead overcoordinated Si atoms with five nearest-neighbor atoms are the microscopic origin for the main coordination defect state in amorphous silicon.[11] Pantelides also coined the name "floating bond" for this defect. A brief comparison between the predicted qualitative properties of dangling bonds and floating bonds is given in Table I. According to Table I, for a distinction between these two types of defects in amorphous silicon, it is necessary to obtain a detailed picture of the electronic wave function, especially a quantitative measure for the defect localization and the state of hybridization. In principle, this information can be obtained from a correct analysis of the ^{29}Si hyperfine structure of the $g=2.0055$ defect resonance in undoped a-Si:H. The observation of this hyperfine structure was first reported in 1986 by the present authors,[12] and it was argued that this structure was indeed compatible with the assignment of the underlying defects to Si dangling bonds.[13] This view was criticized by Pantelides[11] and Stathis and Pantelides,[14] who claimed that the observed hyperfine structure of the $g=2.0055$ ESR spectrum appeared to be more in favor of the floating bond model, instead. Subsequent theoretical investigations by a number of different groups have so far been unable to provide clear evidence for or against either of the two topologically distinct microscopic models.[15–18]

In this paper, we present a careful analysis of the ^{29}Si hyperfine spectrum in undoped a-Si:H containing the natural abundance of the ^{29}Si isotope ($\approx 4.5\%$). This analysis comprises the measurement of the weak ^{29}Si hyperfine satellites with a sufficient signal-to-noise ratio, a quantitative description of the "central" $g=2.0055$ ESR signal due to ^{28}Si and ^{30}Si defects, and the extraction of the ^{29}Si hyperfine parameters via numerical simulation of the hyperfine spectra. In this study we have purposely avoided the use of isotopically (^{29}Si) enriched samples, since our earlier work[12] has shown that high ^{29}Si contents lead to a loss of spectral details in the hyperfine structure because of isotropic interaction with an unknown number of nearest- or second-nearest-neighbor ^{29}Si atoms.

TABLE I. Proposed properties of dangling and floating bonds in amorphous silicon.

	Dangling bond	Floating bond
Crystalline analog	Si vacancy	Si interstitial
Network mobility	low	high
Occurrence in	low-density regions	high-density regions
Chemical notation	$Si^0_{(3)}$	$Si^0_{(5)}$
Charge	0	0
Coordination number	3	5
Orbital type	Atomic orbital (Si sp^3)	Molecular orbital
Localization	strong	weak
Energy level	midgap	midgap
Symmetry	trigonal	?

II. DATA ACQUISITION AND SIMULATION

The samples employed in this study were deposited from undiluted SiH_4 or SiD_4 (with D=deuterium) by a standard rf glow discharge at a substrate temperature of 230 °C. Typical spin densities were about 10^{16} cm^{-3}, so that relatively large sample volumes (≈ 0.1 cm^3) were necessary to obtain a sufficient signal-to-noise ratio. Spin resonance spectra were recorded at room temperature in the X band, using low microwave powers (1 mW) and small field-modulation amplitudes (4 G peak to peak at 100 kHz) in order to prevent artifacts due to saturation and overmodulation. Signal averaging was performed during approximately 4 h with an on-line computer. After each run, the spectrometer background was recorded under the same conditions, but with an empty sample tube.

Numerical simulations of the experimental spectra were performed by assuming a defect wave function with the same axial symmetry for both the g tensor and the hyperfine tensor. The angular dependences of the effective g value g and the hyperfine interaction A can then be approximated by

$$g(Y)=\tfrac{1}{3}(g_{\parallel}+2g_{\perp})+\tfrac{1}{3}Y(g_{\parallel}-g_{\perp}) , \tag{1}$$

$$A(Y)=A_{\rm iso}+YA_{\rm aniso} , \tag{2}$$

where the principal g values $g_{\parallel}$ and $g_{\perp}$ and the isotropic and anisotropic hyperfine interaction constants $A_{\rm iso}$ and $A_{\rm aniso}$ are the input parameters of main interest for the microscopic interpretation of the ESR data. [It should be noted that Eq. (1) for the effective g value is only correct in the limit of small g shifts, $g(Y)-g_0 \ll g_0 = 2.002\,319\ldots$, which is generally the case in a-Si:H.] The variable Y appearing in Eqs. (1) and (2) is determined by the angle θ between the external magnetic field and the defect symmetry axis,

$$Y=3\cos^2\theta-1 . \tag{3}$$

For a random orientation of the defect symmetry axes, the probability density for Y (the "powder pattern") is given by

$$\frac{dN}{dY}\propto(Y+1)^{-1/2} . \tag{4}$$

The ESR intensity versus magnetic field H is then determined by (i) calculating the resonance field H_0 as a function of Y for the central (^{28}Si) resonance [$H_{0,c}=\hbar\omega/\mu_B g(Y)$] and for the two ^{29}Si satellites [$H_{0,\rm HF}=H_0\pm\frac{1}{2}A(Y)$], (ii) convoluting with a suitable Gaussian broadening function

$$F(H-H_0)\propto W^{-1}\exp\left[-\ln 2\left[\frac{H-H_0}{W}\right]^2\right] \tag{5}$$

(where W represents half-width at half maximum), and finally (iii) summation over all values of Y according to the powder pattern Eq. (4) and taking into account the natural abundance of ^{29}Si.

In general, the width W of the shape function F in Eq. (5) will be an unknown function of the angular parameter Y. In the present paper we have assumed that there are two contributions to W, one coming from the g-tensor anisotropy,[4] and a second one accounting for random fluctuations of the hyperfine interaction constant $A(Y)$. Both contributions (for reasons which are discussed below) are approximated by linear functions of Y

$$W_i(Y)=W_{i,0}+Y\,\Delta W_i , \tag{6}$$

where the index i denotes either the g tensor or the hyperfine tensor contribution. In the case of the central (^{28}Si) resonance, only the g-tensor contribution has to be considered, whereas for the simulation of the ^{29}Si hyperfine satellites both contributions need to be taken into account. In this latter case, we have calculated the effective width $W(Y)$ of the line-shape function F in Eq. (5) via the geometric mean of the two components in Eq. (6), as appropriate for statistically independent Gaussians,

$$W^2(Y)=\sum_i W_i^2(Y) . \tag{7}$$

III. RESULTS AND DISCUSSION

A. The central resonance

We begin with a discussion of those defects in undoped a-Si:H which are localized at ^{28}Si or ^{30}Si nuclei with nuclear spin $I=0$ and, therefore, do not experience a

resolved hyperfine interaction. The corresponding spin resonance signal is the usual ESR line with an effective g value $g=2.0055$ and is shown by the solid curve in Fig. 1(a). This spectrum is found to be the same for a-Si:H prepared under a large variety of conditions and for spin densities from 10^{15} to 10^{18} cm^{-3}. In addition to its g value, the spectrum is characterized by a peak-to-peak linewidth of $\Delta H \approx 8$ G which is mainly due to g-value anisotropy,[19,20] and by a specific asymmetric line shape of the ESR derivative signal: The amplitude of the high-field peak is about 10% larger than that of the low-field peak. The simulation of this spectral line shape is possible with the following set of parameters:

$$g_{\parallel}=2.004, \quad W_{\parallel}=3.8 \text{ G}, \qquad g_{\perp}=2.008, \quad W_{\perp}=5.0 \text{ G}. \tag{8}$$

Here, $\parallel$ and $\perp$ refer to the cases $\theta=0°$ and 90° in Eq. (3), respectively. The unbroadened powder pattern [Eq. (4)] corresponding to these principal values of an axially symmetric g tensor is shown in Fig. 1(b). Broadening of this powder pattern by Gaussian functions whose half widths at half maximum increase linearly from $W_{\parallel}$ to $W_{\perp}$ as the g value increases from $g_{\parallel}$ to $g_{\perp}$ yields the theoretical ESR derivative indicated by the dotted curve in Fig. 1(a). The broadening W is taken to be linearly proportional to the g shift $g(Y)-g_0$, because the g shift is a measure for the spin-orbit coupling. The greater the coupling, the more sensitive the site should be to local fluctuations of the defect orbital. The agreement with the experimental curve is satisfactory except for the extreme wings of the resonance line. The fitting procedure is made easy by the fact that a variation of the different parameters in (8) has quite separate influences on the calculated line shapes. Thus, the position of the low-field peak depends mostly on $g_{\perp}$, the peak-to-peak linewidth is given by the anisotropy $g_{\parallel}-g_{\perp}$, and the line-shape asymmetry (which is opposite to what could be expected from the unbroadened powder pattern) is almost entirely determined by the ratio $W_{\parallel}/W_{\perp}$. This "orthogonality" of the effect of the fitting parameters on the final line shape ensures that all four parameters can be determined within a reasonable accuracy (±5%).

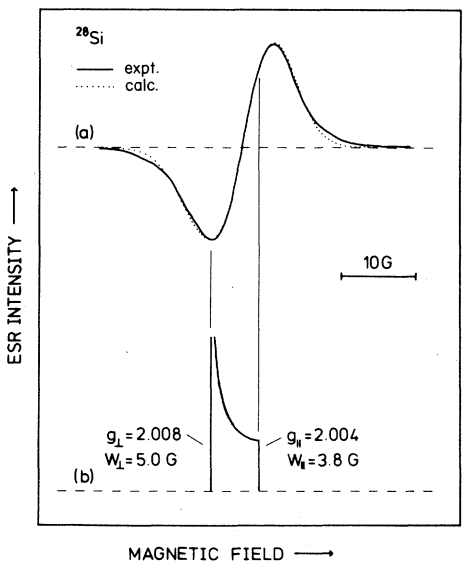

FIG. 1. Experimental (solid curve) and theoretical (dotted curve) line shape of the $g=2.0055$ spin resonance signal in undoped a-Si:H. (b) shows the underlying powder pattern of the g tensor, with principal values $g_{\parallel}=2.004$ and $g_{\perp}=2.008$. $W_{\parallel}$ and $W_{\perp}$ are the half-widths at half maximum of the Gaussian broadening functions used in the line-shape simulation.

From a microscopic point of view, we note that the obtained fitting parameters in a-Si:H are in agreement with Si dangling-bond defects in other systems.[21] In particular, similar values of $g_{\parallel}$ and $g_{\perp}$ have been observed for SiH_3 radicals trapped in Kr matrices at low temperatures ($g_{\perp}=2.007$, $g_{\parallel}=2.003$). Moreover, our value of $g_{\perp}\approx 2.008$ agrees well with experimental data for Si dangling-bond defects at Si/SiO_2 interfaces.[4]

B. ^{29}Si hyperfine satellites

In Fig. 2, we show the ESR spectrum of the same sample as in Fig. 1, however with a sensitivity increased by a factor of 100 and the magnetic field scale expanded by a factor of 4. Under these conditions, two new resonance signals can be observed on the left- and the right-hand side of the central resonance. These two signals are the hyperfine spectra of those defects which are localized on ^{29}Si nuclei. ^{29}Si is a silicon isotope with a nuclear spin $I=\frac{1}{2}$ and a natural abundance of 4.7 at. %. The assignment of the satellite lines in Fig. 2 to ^{29}Si hyperfine states has been corroborated by ^{29}Si enrichment studies reported earlier.[12] Similar hyperfine lines have also been seen in electron-nuclear double resonance (ENDOR) investigations of undoped a-Si:H.[22,23]

A second possible hyperfine nucleus which is present in intrinsic a-Si:H with considerable concentrations is ^{1}H ($I=\frac{1}{2}$, 100% natural abundance). In order to check for any contributions of proton spins to the hyperfine struc-

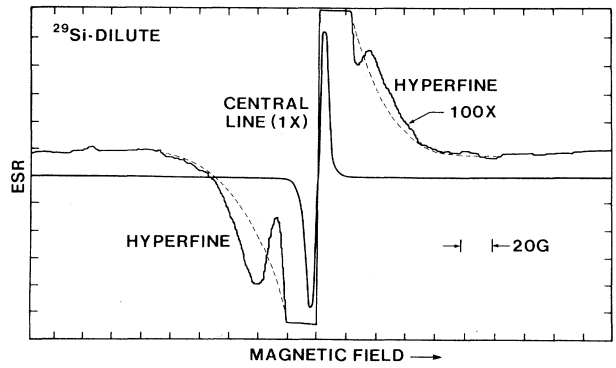

FIG. 2. ^{29}Si hyperfine structure of the $g=2.0055$ resonance in a-Si:H containing the natural abundance of the ^{29}Si isotope. The central line corresponds to the experimental curve in Fig. 1(a).

ture of the $g=2.0055$ resonance, we have also investigated the ESR response of deuterated amorphous silicon a-Si:D obtained from deposition of SiD_4. As demonstrated in Fig. 3, a-Si:D exhibits a ^{29}Si hyperfine spectrum virtually identical to that of a-Si:H, thus excluding any first-order effect of H or D on the hyperfine structure of the $g=2.0055$ resonance.

A very important feature of the ^{29}Si hyperfine spectra in Figs. 2 and 3 which will be exploited in the following is the pronounced asymmetry of the two hyperfine satellites. In the derivative ESR spectra displayed, the low-field (left) satellite is clearly distinguishable from the central resonance, whereas the high-field (right) satellite has a much smaller peak-to-peak amplitude and seems to extend over a wider magnetic field range. This qualitative difference between the two hyperfine lines can be easily explained on the basis of Eqs. (1)–(4). According to Eq. (1), the effective hyperfine splitting $A(Y)$ will be maximal for $Y=2$ ($\theta=0°$),

$$A_{\max}=A_{\parallel}=A_{\rm iso}+2A_{\rm aniso}\ . \tag{9a}$$

The minimum value of $A(Y)$ is obtained for $\theta=90\%$, $Y=-1$,

$$A_{\min}=A_{\perp}=A_{\rm iso}-A_{\rm aniso}\ . \tag{9b}$$

For an axially symmetric hyperfine tensor, the probability density of a given splitting between $A_{\parallel}$ and $A_{\perp}$ will be distributed according to Eq. (4), i.e., it will diverge for $A_{\perp}$ ($Y=-1$). This situation is shown in the upper part of Fig. 4. In addition to the hyperfine splitting, one also has to take into account the anisotropic g shift in order to determine the final resonance line shape. Again, for an axially symmetric g tensor, the g values will be distributed between $g_{\parallel}$ and $g_{\perp}$, with a divergence at $g_{\perp}$ [cf. Eq. (1) and Fig. 1]. This is depicted in the middle part of Fig. 4. The final powder pattern for the two hyperfine satellites are now obtained by adding the g shift and the hyperfine splitting, as seen in the lower portion of Fig. 4. The result is a narrowing of the left satellite, since here the effects of the g tensor and hyperfine tensor anisotropies have different signs, whereas the right satellite ex-

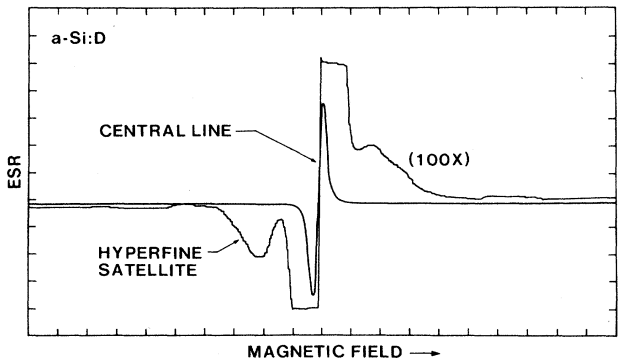

FIG. 3. Same spectra as in Fig. (2), but for deuterated amorphous silicon a-Si:D.

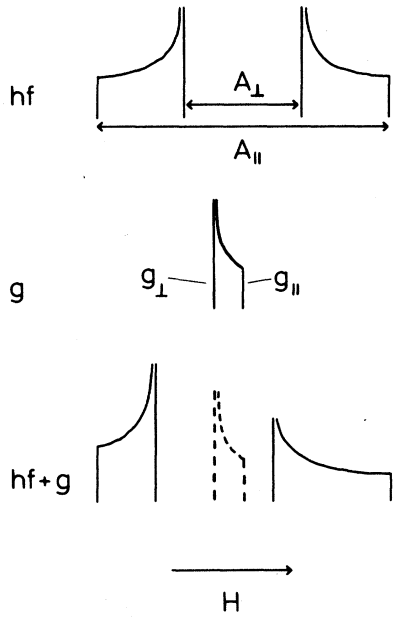

FIG. 4. Theoretical powder patterns caused by the hyperfine and g tensors of randomly oriented, axially symmetric paramagnetic defects: hyperfine tensor powder pattern (hf), g-tensor powder pattern (g), and combination of both (hf+g).

periences a broadening due to the additive superposition of the anisotropy contributions. In a-Si:H, the g anisotropy in the X band according to Fig. 1 amounts to about 6.5 G, so that we can expect the widths of the two ^{29}Si hyperfine absorption spectra to differ by at least 13 G.

Experimentally, the main difficulty in determining the ^{29}Si hyperfine line shape is the low natural abundance of ^{29}Si. In principle, it would be possible to improve this situation by using isotopically enriched a-Si:H, but our previous measurements have shown that this also leads to an additional broadening mechanism due to unresolved hyperfine interaction between the $g=2.0055$ defect state and the nearest- or second-nearest-neighbor ^{29}Si atoms. The probability of occurrence of these nuclei will increase very rapidly with the concentration of ^{29}Si, so that the observation of the unperturbed ^{29}Si hyperfine interaction is essentially restricted to the dilute case encountered in a-Si:H with the natural abundance of ^{29}Si. Thus, for the experimental determination of the hyperfine line shapes an essential point is the correct subtraction of the central resonance in Fig. 2 or 3. This would require the knowledge of the central resonance line shape in the region of the hyperfine satellites with an accuracy of about 10^{-3} times the central resonance amplitude, which is far beyond the accuracy of any realistic simulation. Thus, other ways have to be used for the subtraction of the central resonance background in the experimental spectra. For the present case, we have adopted the following procedure. The background was chosen as a smooth, structureless curve which joins the experimental derivative spectra continuously and with the same slope on both sides of either hyperfine satellite. Here, structureless

means that the background curve decreases in a monotonic manner away from the resonance center, with no structure occurring in the second derivative over the region of the hyperfine satellites. The resulting background was accepted when after subtraction (i) the first integral of the hyperfine derivative spectra (i.e., the real absorption spectra) returned to zero for each hyperfine satellite separately, and (ii) the second integral (i.e., the satellite spin density) agreed to within better than 10% between the two satellites. The entire procedure was tested on three different experimental spectra, including the two for which the result of the central-line subtraction is shown by the solid curves in Figs. 5(a) and 5(b). In all three cases the obtained hyperfine spectral shapes agreed reasonably, with some differences occurring only in the high-field wing of the right-hand satellite. For further comparison, the first integral of the experimental spectra in Fig. 5(a), is shown in 5(c), where the relative values I of the second integral (i.e., the relative spin density corresponding to each satellite) are also indicated.

The dotted curves in Fig. 5 indicate the results of the line-shape simulation. For this simulation, the fitting parameters, Eq. (8), of the central resonance were adopted in order to correctly account for the g-tensor anisotropy and broadening. The only additional fitting parameters were the isotropic and anisotropic hyperfine constants $A_{\rm iso}$ and $A_{\rm aniso}$, and an anisotropic hyperfine broadening

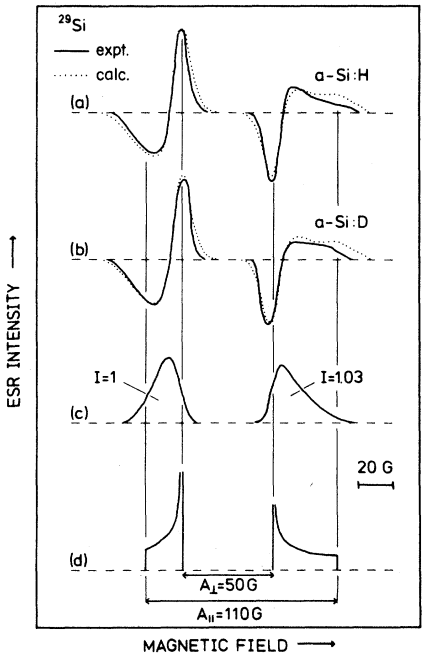

FIG. 5. ^{29}Si hyperfine spectra deduced from the experimental curves in Figs. 2 and 3. Solid and dotted curves in (a) and (b) denote experimental and simulated line shapes, respectively. Solid curves in (c) are the integral of the spectra in (a). "I" is the relative, integrated spin density of each hyperfine satellite. The powder pattern used for the line-shape simulation is indicated in (d).

width which was allowed to increase from $W_\parallel$ to $W_\perp$ with increasing Y [cf. Eq. (3)] as in the case of the g tensor. The microscopic origin for this broadening of the hyperfine interaction constants lies in the fluctuations of the localization and s-p hybridization of the $g=2.0055$ defects in a disordered environment. As before, we assume here that these fluctuations will lead to a larger broadening the larger the effective hyperfine coupling constant $A(Y)$ in Eq. (2). The calculated curves in Fig. 5 were obtained for the following set of parameters:

$$A_{\rm iso}=70\ {\rm G},\quad W_\parallel=10\ {\rm G}\ ,$$
$$A_{\rm aniso}=20\ {\rm G},\quad W_\perp=5\ {\rm G}\ . \tag{10}$$

The corresponding values for $A_\parallel$ and $A_\perp$ are, according to Eq. (9), $A_\parallel=110$ G and $A_\perp=50$ G. These values are shown in Fig. 5(d), together with the theoretical, unbroadened hyperfine powder pattern underlying the experimental curves in 5(a). It should be noted that, as in the case of the central resonance simulation, the different fitting parameters of the hyperfine satellites have characteristic influences on the obtained line shapes. Thus, $A_{\rm iso}$ and $A_{\rm aniso}$ are mainly reflected by the field position of the extrema and zero crossings of the resonances, whereas $W_\parallel$ and $W_\perp$ mainly influence the relative height of the extrema. This allows us to place the hyperfine coupling constants within the following limits: $A_{\rm iso}=72\pm3$ G, $A_{\rm aniso}=18\pm3$ G. In particular, we can exclude the estimate $A_{\rm aniso}<8$ G given in Ref. 14. This estimate was based on the peak-to-peak width of the hyperfine absorption derivative or on the width of the integral spectrum obtained by H-ENDOR detected ESR. However, it is known from the literature, e.g. Ref. 24, that this may severely underestimate the true anisotropic width of the underlying powder pattern. This fact is already obvious from Fig. 5: Taking the average peak-to-peak width of the two satellites in (a) or the average FWHM in (c) we would indeed obtain values for $A_{\rm aniso}$ between 8 and 12 G, whereas the true anisotropy in (d) is 20 G.

C. Microscopic defect structure

Having determined the g tensor and hyperfine parameters of the $g=2.0055$ resonance, one would now like to translate these results into properties of the corresponding defect wave function $|D\rangle$. The most commonly employed procedure to do this has been proposed by Watkins and Corbett[25] and makes use of the linear combination of atomic orbitals (LCAO) expansion of $|D\rangle$,

$$|D\rangle=\sum_i \alpha_i(\sigma_i|s\rangle+\pi_i|p\rangle)\ , \tag{11}$$

where $|s\rangle$ and $|p\rangle$ denote the atomic $3s$ and $3p$ orbitals of Si, i indexes all atoms within the extent of the wave function $|D\rangle$, and the projection coefficients α_i, σ_i, and π_i obey the normalization conditions $\sum_i\alpha_i^2=1$, $\sigma_i^2+\pi_i^2=1$ for all i. For a strongly localized wave function, usually one atom in Eq. (11) will contribute more to the sum than the rest of the atoms, and this center of localization will be given the index $i=0$. It is then possible to determine

α_0, σ_0, and π_0 from the experimental hyperfine constants through the relations

$$\alpha_0^2\sigma_0^2 = A_{\text{iso}}/A(s) ,$$
$$\alpha_0^2\pi_0^2 = A_{\text{aniso}}/A(p) , \quad (12)$$
$$\sigma_0^2+\pi_0^2 = 1 ,$$

where $A(s)$ and $A(p)$ are the hyperfine constants for pure $|s\rangle$ and $|p\rangle$ orbitals, respectively. To the extent that further interaction constants can be resolved, e.g., by ENDOR measurements, it is possible to also determine coefficients for nearest, next-nearest, . . . , neighbors and thus to map out the defect wave function.

The LCAO approach as described above has two problems. First, it requires the knowledge of the atomic interaction constants $A(s)$ and $A(p)$ of the atoms in question, i.e., silicon in our case. Except for the cases where they have been determined experimentally, the atomic hyperfine constants are usually calculated from Hartree-Fock orbitals. Different values for $A(s)$ and $A(p)$ used in the literature for ^{29}Si are listed in Table II.[25–27] For the following discussion, we will use the values given in Ref. 25, namely, $A(s)=1490$ G and $A(p)=36$ G, since these are the numbers most commonly employed for the defect analysis in crystalline Si. Besides, they correspond roughly to the average of the interaction constants in Table II. However, it is obvious from this table that the constants which are used for the hyperfine data reduction according to Eq. (12) vary by as much as 30% among different authors. This makes a direct comparison uncertain, especially as far as the localization parameter α_0 in Eq. (12) is concerned.[28] [Since the ratios $A(s)/A(p)$ in Table II are approximately the same, the hybridization parameters σ_0 and π_0 are much less affected.]

The second problem of the LCAO approach is that it identifies the net charge density of the paramagnetic defect wave function with the net spin density. As pointed out recently by Cook and White,[29] this identification can break down mainly because of two resons: (i) the unpaired spin in the valence orbitals can produce a nonzero spin density in atomic core levels, thus causing additional hyperfine splittings not accounted for by the simple LCAO picture (spin polarization), and (ii) the bonding interaction within an atomic cluster may perturb the shape of the pure $|s\rangle$ and $|p\rangle$ orbitals, so that estimates for $A(s)$ and $A(p)$ obtained for isolated atoms may not be correct for the same atoms embedded in a solid matrix. For the case of Si dangling bonds at the crystalline Si/SiO_2 interface, Cook and White have shown that a more sophisticated analysis may indeed differ from the LCAO picture significantly, especially as far as an estimate of the amount of s character σ_0^2 on the central atom is concerned.

However, for our case of the $g=2.0055$ resonance in amorphous silicon, both deficiencies of the simple LCAO analysis are less disturbing in view of the larger error bars of the experimentally determined hyperfine constants, and as long as we are only attempting a semiquantitative description of the defect state. With this caveat in mind, we can calculate the following projection coefficients $(\alpha_0,\sigma_0,\pi_0)$ from the experimental data and the LCAO relations, Eq. (12),

$$\alpha_0^2 = 0.45-0.65 ,$$
$$\sigma_0^2 = 0.07-0.11 , \quad (13)$$
$$\pi_0^2 = 0.89-0.93 .$$

This set of parameters is the characteristic signature of a silicon dangling-bond defect, as it has been observed in many other systems.[21] The hybridization of $\approx 10\%$ s character and $\approx 90\%$ p character indicates that the central Si atom has relaxed back towards the three nearest-neighbor atoms to form an almost planar structure. [In fact, according to the more sophisticated analysis in Ref. 29, σ_0^2 in Eq. (13) should only be regarded as an upper limit for the true s character of the defect wave function.] About half of the wave function is localized at the central atom, with the remaining charge density distributed onto the nearest- and next-nearest-neighbor atoms. From our earlier work on ^{29}Si-enriched specimens[12] we know that the wave-function overlap with the neighboring atoms produces a superhyperfine interaction of about 25 G, requiring that about 10% of the total defect charge density is localized on a sp^3 hybrid of at least one Si neighbor. This is entirely compatible with the estimate $\alpha_0^2 \leq 65\%$ for the charge density on the central atom. A similar superhyperfine interaction has also been observed for dangling bonds at the Si/SiO_2 interface,[4,29,30] with a magnitude of approximately 15 G. Thus, we may conclude that the $g=2.0055$ defect state in amorphous silicon is structurally very similar to the P_b defect at the Si/SiO_2 interface, which is probably the most studied example of a Si dangling bond. The main difference between these two defects is their degree of localization on the central

TABLE II. Hyperfine interaction constants for $3s$ and $3p$ atomic orbitals of ^{29}Si (equivalence between the units: 1 G=2.802 MHz=9.346×10^{-5} cm^{-1}).

$A(s)$ (G)	$A(p)$ (G)	Refs.
1640	40.5	26
1490	36.0	25
1206	31.0	4,27

TABLE III. Experimental and theoretical (Refs. 31 and 32) ESR parameters for the $g=2.0055$ resonance in amorphous silicon (SHF, superhyperfine interaction; α_0^2, localization parameter).

Parameter	Experiment	Theory
$g_\parallel$	2.004	2.003
$g_\perp$	2.008	2.008
A_{iso}	70–75 G	70–110 G
A_{aniso}	15–20 G	13–20 G
SHF	20–30 G	5–30 G
α_0^2	0.45–0.65	0.48–0.73

atom: $\alpha_0^2 \approx 0.55$ in a-Si:H versus $\alpha_0^2 = 0.7$ at the c-Si/SiO_2 interface.

A second possible way to demonstrate the dangling-bond character of the $g = 2.0055$ defect in a-Si:H which does not rely on the LCAO analysis employed above is to compare the experimental raw data with predictions of model calculations for dangling-bond defects. Such calculations have actually been performed by Ishii and coworkers long before the ^{29}Si hyperfine structure in a-Si:H was observed experimentally.[31,32] The comparison in Table III demonstrates the good quantitative agreement between experiment and theory, thereby giving additional support to the dangling-bond model.

IV. CONCLUSION

We have performed a detailed investigation of the $g = 2.0055$ resonance in amorphous silicon, with special emphasis on the ^{29}Si hyperfine interaction in samples with the low, natural ^{29}Si isotope concentration. The principal components of the g tensor and the hyperfine tensor were obtained by computer simulations of the central resonance and the hyperfine satellite line shapes. We obtain values of $g_\parallel = 2.004$, $g_\perp = 2.008$, $A_{iso} = 73 \pm 3$ G, and $A_{aniso} = 18 \pm 3$ G for the g-tensor components and the isotropic and anisotropic hyperfine constants, respectively. These results agree quantitatively with predictions from previous calculations for Si dangling-bond defects. A simple LCAO analysis of the hyperfine constants shows that the underlying defect wave function is mostly localized on one Si atom and has almost pure p character. The structural parameters deduced for the $g = 2.0055$ defect agree very well with those of Si dangling bonds at the Si/SiO_2 interface. We are, therefore, led to the conclusion that there are no compelling reasons to abandon the dangling-bond picture of the principal defect state in amorphous silicon. On the contrary, in conjunction with recent calculations of the electronic structure of overcoordinated silicon atoms[15,16] our results suggest that the ^{29}Si hyperfine structure is actually incompatible with the floating bond model. According to these calculations, a floating bond wave function has much less weight on any Si atom than a dangling-bond state, due to the delocalized nature of a floating bond. Thus, Fedders *et al.* find less than 25% of the total wave function on a given Si atom, which is a factor of 2 smaller than the lower limit obtained in our analysis.

ACKNOWLEDGMENTS

One of us (M.S.) would like to thank his colleagues at Xerox Palo Alto Research Center for their hospitality and inspiration during this work.

[1] M. Brodsky and R. S. Title, Phys. Rev. Lett. **23**, 581 (1969).
[2] P. C. Taylor, in *Semiconductors and Semimetals,* edited by J. I. Pankove (Academic, New York, 1984), Vol. 21C, p. 99.
[3] M. Taniguchi, M. Hirose, Y. Osaka, S. Hasegawa, and T. Shimizu, Jpn. J. Appl. Phys. **19**, 665 (1980).
[4] K. L. Brower, Appl. Phys. Lett. **43**, 1111 (1983).
[5] D. Adler, J. Phys. (Paris) Colloq. **42**, C4-3 (1981).
[6] Y. Bar-Yam and J. D. Joannopoulos, Phys. Rev. Lett. **56**, 2203 (1986).
[7] R. A. Street, J. Kakalios, and T. M. Hayes, Phys. Rev. B **34**, 3030 (1986).
[8] G. Müller, Appl. Phys. A **45**, 103 (1988).
[9] M. Stutzmann, Philos. Mag. B **56**, 63 (1987).
[10] Z. E. Smith and S. Wagner, Phys. Rev. Lett. **59**, 688 (1986).
[11] S. T. Pantelides, Phys. Rev. Lett. **57**, 2979 (1986).
[12] D. K. Biegelsen and M. Stutzmann, Phys. Rev. B **33**, 3006 (1986).
[13] M. Stutzmann and D. K. Biegelsen, Phys. Rev. Lett. **60**, 1682 (1988).
[14] J. H. Stathis and S. T. Pantelides, Phys. Rev. B **37**, 6579 (1988).
[15] P. A. Fedders and A. E. Carlson, Phys. Rev. B **37**, 8506 (1988).
[16] N. Ishii and T. Shimizu, Jpn. J. Appl. Phys. Pt. 2 **27**, L1800 (1988).
[17] L. Martin-Moreno and J. A. Vergés, Phys. Rev. B **39**, 3445 (1989).
[18] M. Cook and C. T. White, Phys. Rev. Lett. **59**, 1741 (1987).
[19] H. Dersch, J. Stuke, and J. Beichler, Phys. Status Solidi B **107**, 307 (1981).
[20] M. Stutzmann and J. Stuke, Solid State Commun. **47**, 635 (1983).
[21] M. Stutzmann, Z. Phys. Chem. **151**, 211 (1987).
[22] S. Yamasaki, S. Kuroda, and K. Tanaka, in *Stability of Amorphous Silicon Alloy Materials and Devices,* Proceedings of an International Conference on Stability of Amorphous Silicon Alloy Materials and Devices, AIP Conf. Proc. No. 157, edited by B. L. Stafford and E. Sabisky (AIP, New York, 1987), p. 9.
[23] H. Yokomichi, I. Hirabayashi, and K. Morigaki, Solid State Commun. **61**, 697 (1987).
[24] M. M. Malley, J. Mol. Spectrosc. **17**, 310 (1965).
[25] G. D. Watkins and J. W. Corbett, Phys. Rev. **134**, A1359 (1964).
[26] J. R. Morton and K. F. Preston, J. Magn. Res. **30**, 577 (1978).
[27] J. R. Morton, Chem. Rev. **64**, 453 (1964).
[28] It is interesting to note that the lowest values in Table II, $A(s) = 1206$ G and $A(p) = 31$ G, are generally used for dangling-bond defects at the Si/SiO_2 interface. As a consequence, the localization parameter α_0 for these defects deduced from ^{29}Si hyperfine data will be systematically larger by about 20%.
[29] M. Cook and C. T. White, Phys. Rev. B **38**, 9674 (1988).
[30] W. E. Carlos, Appl. Phys. Lett. **50**, 1450 (1987).
[31] N. Ishii, M. Kumeda, and T. Shimizu, Jpn. J. Appl. Phys. Pt. 2 **20**, L673 (1981); **20**, L920 (1981).
[32] N. Ishii, M. Kumeda, and T. Shimizu, Phys. Status Solidi B **116**, 91 (1983).